



Microstructure Effects on Effective Gas Diffusion Coefficient of Nanoporous Materials

Yangyu Guo¹ · Xinting He¹ · Wenzheng Huang¹ · Moran Wang¹ 

Received: 28 December 2017 / Accepted: 25 September 2018 / Published online: 3 October 2018
© Springer Nature B.V. 2018

Abstract

In this work, we develop a numerical framework for gas diffusion in nanoporous materials including a random generation-growth algorithm for microstructure reconstruction and a multiple-relaxation-time lattice Boltzmann method for solution of diffusion equation with Knudsen effects carefully considered. The Knudsen diffusion is accurately captured by a local diffusion coefficient computed based on a corrected Bosanquet-type formula with the local pore size determined by the largest sphere method. A robust validation of the new framework is demonstrated by predicting the effective gas diffusion coefficient of microporous layer and catalyst layer in fuel cell, which shows good agreement with several recent experimental measurements. Then, a detailed investigation is made of the influence on effective gas Knudsen diffusivity by many important microstructure factors including morphology category, size effect, structure anisotropy, and layering structure effect. A widely applicable Bosanquet-type empirical relation at the Darcy scale is found between the normalized effective gas diffusion coefficient and the average Knudsen number. The present work will promote the understanding and modeling of gas diffusion in nanoporous materials and also provide an efficient platform for the optimization design of nanoporous systems.

Keywords Effective diffusion coefficient · Knudsen diffusion · Nanoporous material · Lattice Boltzmann method

1 Introduction

Gas diffusion is a transport phenomenon driven by the species concentration difference (Bird et al. 2002). The classical Fick's law describes well the diffusion behavior in molecular diffusion regime where the pore characteristic length is much larger than the gas mean free path (MFP). When the pore characteristic length reduces to be comparable to or even smaller than the gas MFP, the effect of Knudsen diffusion plays a significant role and the Fick's law is no longer valid (Bird et al. 2002). The gas Knudsen diffusion in nanoporous media widely

Yangyu Guo and Xinting He have contributed equally to this work.

✉ Moran Wang
mrwang@tsinghua.edu.cn

¹ Department of Engineering Mechanics and CNMM, Tsinghua University, Beijing 100084, China

exists in many novel energy systems and technology (Kärger et al. 2012), such as the fuel cell as a kind of promising portable power technology which directly converts chemical energy into electricity in an efficient way (Ellis et al. 2001). In the archetypical hydrogen–oxygen proton exchange membrane fuel cell (PEMFC), the electrode is made of three adjacent layers: gas diffusion layer (GDL), microporous layer (MPL) and catalyst layer (CL) (Zamel and Li 2013). The performance of PEMFC is limited by the supply of oxygen which reaches the CL via diffusion through the GDL and MPL successively. As the average pore diameter of MPL and CL is about 100 nm reaching the order of magnitude of air molecule MFP (about 70 nm at room temperature and 1 atm) (Inoue et al. 2016), the gas Knudsen diffusion is an important mechanism therein (Yang et al. 2016). Therefore, an accurate description of gas diffusion in nanoporous materials is crucial to promote the optimization design of these novel energy systems and technologies.

In recent years, there are some important advances in experimental measurement of effective gas diffusivity in nanoporous MPL and CL structures (Inoue et al. 2016; Yu and Carter 2010; Chan et al. 2012; Yu et al. 2012). To explain the underlying physical mechanism, there are mainly two categories of theoretical and numerical methods at different levels of description (Zamel and Li 2013; Yuan and Sunden 2014): (1) the direct pore-scale method based on the local quantities in the pore and (2) the effective method at Darcy scale based on the averaged quantities over the representative elementary volume (REV) of porous media (Kaviany 1995). The effective method at Darcy scale provides a relation between the effective gas diffusivity and macroscopic statistical parameters (porosity, tortuosity, et al.) of the nanoporous structures. Here the ‘statistical’ means ‘statistical averaging over the REV of porous media.’ An analytical fractal model was presented for gas diffusion through fibrous nanoporous structures including both the Fickian and Knudsen diffusion (Shou et al. 2014). This fractal model remains to be validated for more complex fibrous structures beyond the highly anisotropic webs and GDLs. In a recent work (Andisheh-Tadbir et al. 2015), the MPL is modeled as a periodic structure with the unit cell containing two domains: the large pore and the surrounding agglomerates. The effective gas diffusion coefficient of MPL is derived from an analogy to the effective thermal conductivity of a similar periodic structure. Some multiscale models with inputs from more refined scale than Darcy scale have been also developed. Becker et al. (2011), Zamel et al. (2012) proposed a mathematical model based on the Bosanquet empirical formula at the Darcy scale, with the effective Fickian diffusivity and Knudsen diffusivity obtained, respectively, from pore-scale simulation and molecular dynamics simulation. Inoue et al. (2016), Inoue and Kawase (2016a) computed the relative gas diffusion coefficient of MPL and CL structures as the ratio of porosity to tortuosity with a correction considering the Knudsen diffusion, where the tortuosity was determined by a random-walk method. Although the effective method at Darcy scale provides a fast avenue to estimate the effective diffusivity of a nanoporous medium, it has often neglected the influence of some important pore-scale microstructure details.

For a deeper understanding of the mechanism of gas diffusion through nanoporous structures, pore-scale simulations have been extensively done in the past years. There exist mainly two categories of pore-scale numerical approaches: (1) the stochastic method, i.e., Monte Carlo (MC) scheme; (2) the deterministic methods including finite volume method (FVM), finite element method (FEM), and lattice Boltzmann method (LBM). As early as in 1990s, Tomadakis and Sotirchos (1991, 1993) used the random-walk MC method to predict the effective Knudsen diffusivity of fibrous structures, which was found to be strongly influenced by the directionality of the fibers. The random-walk MC method was later applied to compute the effective gas diffusivity in sphere-packing nanocomposite porous media (Berson et al. 2011). Some other works have modeled the gas diffusion through a single pore or a combination of

different pore geometries (Galinsky et al. 2014), and the highly porous nanoparticle layers (Dreyer et al. 2014) by the direct simulation Monte Carlo (DSMC) method. Most of the MC studies have considered the gas diffusion in nanoporous media with simple geometries. On the other hand, the MC simulation is inherent with large fluctuations in the near-continuum regime, the reduction of which requires a very large number of particles and huge computational cost. Thus, Lange et al. (2010, 2011, 2012) have developed a numerical framework consisting of an algorithm to reconstruct the nanoporous structure and a FVM solution of diffusion equation to model gas diffusion through the CL structure in PEMFC. The numerical results of effective gas diffusivity are considerably higher than the experimental data mainly due to the inadequate description of the morphology of CL structure (Singh et al. 2014). Such a numerical framework (Lange et al. 2010) has been recently applied to model gas diffusion through MPL structure (El Hannach et al. 2015), where the influence of three microstructure parameters on effective diffusivity is studied. A similar approach was also developed by using experimental methods to obtain the digital image of CL (Litster et al. 2013) or MPL (Nanjundappa et al. 2013) structure, with the diffusion equation solved by FEM-based COMSOL packages. This kind of approach may be limited by the digital resolution of scanning devices, the high cost and the difficulty for optimization design problems.

In contrast to the classical numerical methods (FVM or FEM) for solution of diffusion equation, LBM is an efficient mesoscopic method which holds two advantages (Chen and Doolen 1998; Wang and Pan 2008): (1) a simple treatment of complex boundary conditions based on the standard bounce-back scheme and (2) an easy realization of parallelized computation attributed to the local characteristic of calculation. Two main branches of LBM model together with the structure reconstruction algorithm were developed to simulate gas diffusion in nanoporous materials, including the higher-order multicomponent LBM (Joshi et al. 2007; Kim et al. 2009; Kim and Pitsch 2009; Ma and Chen 2015) and the single-component single-relaxation-time (SRT) LBM (Zhang et al. 2014; Chen et al. 2015; Hussain et al. 2015). The higher-order multicomponent LBM is an extension of the kinetic theory-based LBM for the binary diffusion (Luo and Girimaji 2003) or ternary diffusion (Joshi et al. 2007) with a larger number of discrete lattice velocities (D2Q16 or D3Q64) (Kim et al. 2009; Kim and Pitsch 2009), or with additional artificial collision term (Ma and Chen 2015), or with calibration from the dusty gas model (Joshi et al. 2007) to capture the effect of Knudsen diffusion. Although the higher-order multicomponent LBM was validated for gas diffusion in straight channels (Joshi et al. 2007; Kim et al. 2009; Ma and Chen 2015) or simple porous media (Ma and Chen 2015) at a finite Knudsen number, it remains to be verified for diffusion in complex nanoporous structures within a larger range of transport regimes. The other branch is based on the SRT-LBM for diffusion equation, with the local diffusion coefficient determined by the empirical Bosanquet formula (Zhang et al. 2014; Chen et al. 2015; Hussain et al. 2015). However, the numerical results of effective diffusion coefficient in CL structure were still higher than the experimental data (Chen et al. 2015), which is mainly caused by two possible reasons: (1) the reconstructed CL structure loses some key morphological features of the realistic one; (2) the large variation of Kn leads to unreasonable relaxation time of SRT-LBM for predicting effective diffusivity in pores so that the multiple-relaxation-time (MRT) LBM (d'Humieres et al. 2002; Yoshida and Nagaoka 2010) may become a more suitable choice (Chai et al. 2016).

Therefore, there still lacks an efficient and accurate numerical framework for modeling gas diffusion in nanoporous materials. On the other hand, the previous works have been mainly focused on one or two kinds of nanoporous structures (CL, MPL) for special application. A comprehensive study of microstructure effects on effective gas diffusivity of nanoporous materials remains a challengeable task due to the lack of a robust methodology. The main aim

of the present work is to develop such a numerical framework including a random generation-growth algorithm for structure reconstruction and a MRT-LBM for numerical solution of diffusion equation. The gas diffusion within the entire transition from molecular diffusion regime to Knudsen diffusion regime is captured well by a corrected Bosanquet-type empirical formula. The pore size distribution for computing the local Knudsen number is determined by the largest sphere method (Delerue et al. 1999; Bhattacharya and Gubbins 2006). The remaining of this article is organized below: the mathematical and numerical methods are provided in Sect. 2, with a robust validation through comparison to the results in several experiments in Sect. 3; an extensive numerical study and discussion of the microstructure effects on gas Knudsen diffusion is provided in Sect. 4; concluding remarks are finally made in Sect. 5.

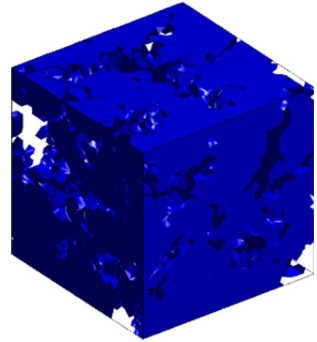
2 Mathematical and Numerical Methods

2.1 Microstructure Reconstruction

2.1.1 Reconstruction of Microporous Layer (MPL) Structure

The MPL structure in PEMFC is an accumulated layer of a primary aggregate of carbon black particles with approximate diameters in the range of 20–50 nm (Inoue et al. 2016). Therefore, the MPL structure can be treated as a kind of granular porous media. The QSGS (Quartet Structure Generation Set) method developed in our previous work (Wang and Pan 2008; Wang et al. 2007) is used to reconstruct the granular MPL structure. The core idea of QSGS method is to reproduce the effective transport properties of the realistic porous medium based on an equivalent porous structure with the macroscopic statistical parameters of the realistic one (Wang et al. 2007). Our algorithm for the generation of porous structures has been widely validated in the prediction of various physical properties (thermal conductivity, electrical conductivity, dielectric permittivity and elastic moduli) of complex porous media as summarized in Ref. Wang and Pan (2008) and has been also demonstrated effective in numerical modeling of diffusion through fibrous and granular structures in our recent study (He et al. 2017). The main line of QSGS method is to grow the chosen growing seed to its neighborhood based on a directional growth probability until the structure reaches the required porosity. The detailed procedure of QSGS method includes five main steps as below (Wang et al. 2007; He et al. 2017): (1) assign a random number by a uniform distribution function within (0, 1) to each grid cell of the computational domain; (2) choose any grid cell whose random number is no greater than the given seed distribution probability s_d as a growing seed; (3) enlarge each growing seed to its neighboring cells in all directions i based on a given directional growth probability matrix D_i ; (4) assign random numbers again to the neighboring cells of the growing seed, and the neighboring cell in direction i will become part of the growing solid phase if its random number is no greater than D_i ; (5) repeat the growing process (1)–(4) until the volume fraction of the solid phase reaches the prescribed value. The three-dimensional schematic of a MPL structure generated by QSGS method with porosity 0.5 is demonstrated in Fig. 1.

Fig. 1 Schematic of granular MPL (microporous layer) structure with porosity 0.5 generated by QSGS (Quartet Structure Generation Set)



2.1.2 Reconstruction of Catalyst Layer (CL) Structure

The CL structure in fuel cells is the cathode made of Pt-nanoparticle catalysts supported on carbon black, and also ionomer as the proton conductor and binder (Inoue et al. 2016; Yu and Carter 2010; Inoue and Kawase 2016a). The diameter of Pt-nanoparticles is at the order of 2–5 nm, whereas the diameter of carbon black particles lies within the range of 20–50 nm, same as that in MPL structure. Therefore, the CL structure can be treated as a kind of granular porous media as well. Although the CL structure has nearly the same backbone as the MPL structure, the introduction of ionomer makes the morphology of CL structure very different from that of the latter. The coating of ionomer may block some pores in CL structure, inferred from the considerably lower porosity measured by MIP (mercury intrusion porosimetry) method than that derived from the structure density (Yu and Carter 2010). The possibly blocked pores are confirmed as the ‘*isolated large pores*’ in later works (Inoue et al. 2016; Inoue and Kawase 2016a; b), where the formation mechanism and their influence on diffusion performance are studied in details with both experimental and numerical techniques. To sum up, the CL structure is a heterogeneous granular porous material with isolated large pores embedded in the MPL-like background structure.

To properly reconstruct the CL structure, it is crucial to determine the ratio of isolated large pore to total pore volume. This ratio is estimated to be 20% from the cumulative pore volume ratio of simulated carbon black aggregate packing with or without large pores in the case of porosity 0.6 (Inoue and Kawase 2016a). Yet there still lacks a method to evaluate the various ratios for CL structure with different porosities. Here, we provide an empirical approach to determine the ratio of isolated large pore in CL structure based on the total porosity. This ratio is calculated from the difference between the measured porosities by MIP method (ε_{MIP}) and by density method ($\varepsilon_{\text{density}}$) through the following formula:

$$R = \frac{\varepsilon_{\text{density}} - \varepsilon_{\text{MIP}}}{\varepsilon_{\text{density}}}. \quad (1)$$

A good linear scaling is found between the ratio of isolated large pore to total pore volume and the total porosity, as shown in Fig. 2a. Thus, the following empirical expression is proposed to correlate the ratio of isolated large pore to the total porosity of CL structure:

$$R = a\varepsilon_{\text{density}} + b, \quad (2)$$

where the non-dimensional coefficients are specified as $a = -1.7658$ and $b = 1.4443$ by fitting the experimental data of CL structures with different porosities (Yu et al. 2012).

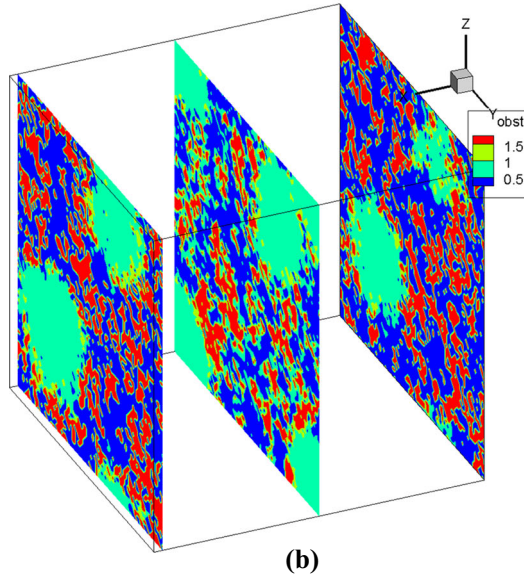
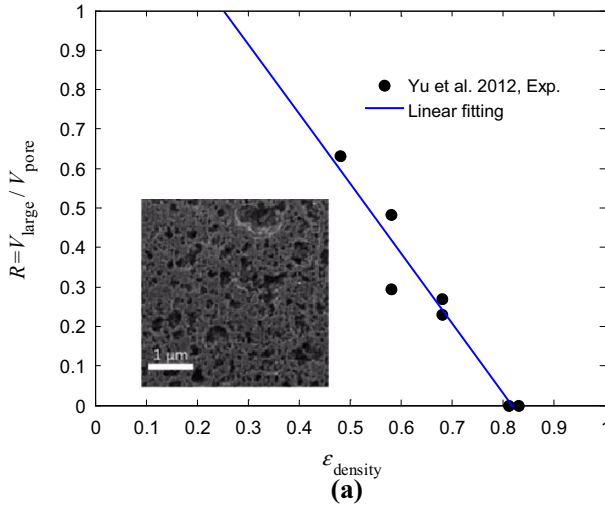


Fig. 2 Ratio of isolated large pore to total pore volume and the schematic of reconstructed CL structure with isolated large pore by QSGS method: **a** ratio of large pore volume to total pore volume versus the porosity calculated from structure density, the filled circles represent the experimental data (Yu et al. 2012), whereas the solid line represents an empirical linear fitting: $R = a\epsilon_{\text{density}} + b$, with $a = -1.7658$ and $b = 1.4443$, the inset figure is the SEM image of isolated large pore in CL structure from the literature (Inoue et al. 2016; Inoue and Kawase 2016a); **b** isolated pore in the generated CL structure, the red part, blue part and green part represent the solid phase, connected pore and isolated pore, respectively

After the ratio of isolated large pore is obtained through Eq. (2), the granular CL structure is generated by the QSGS method. In comparison with previous numerical reconstruction algorithms which consider the carbon black particle, Pt-nanoparticle and ionomer distinguishingly (Inoue and Kawase 2016a; Lange et al. 2010; Chen et al. 2015), we reconstruct the CL

structure as a whole with the key microstructure parameters including porosity and large pore ratio. The present treatment will be shown sufficient to capture the essential structure feature of the CL and its influence on transport property. The porosity ϵ_{micro} of the background granular porous structure is firstly determined from the given total porosity ϵ_{all} ($= \epsilon_{\text{density}}$) and the estimated ratio of isolated large pore R as $\epsilon_{\text{micro}} = (\epsilon_{\text{all}} - R\epsilon_{\text{all}})/(1 - R\epsilon_{\text{all}})$. Then, the background granular material is reconstructed through the same procedures in Sect. 2.1.1 with the porosity ϵ_{micro} . Finally, the isolated pores are randomly generated on the basis of the background granular material through the similar procedures until the total porosity is satisfied. The schematic of the reconstructed CL material with isolated large pores is illustrated in Fig. 2b. The generated digital structure holds the same feature of ‘discrete isolated large pores inside the background granular medium’ as the realistic structure shown in Fig. 2a. On the other hand, it has the same statistical parameters including the background porosity and total porosity as those of the realistic structure. Therefore, the generated CL structure is supposed to reproduce accurately the effective gas diffusivity as will be shown later. For convenience of numerical treatment without losing the real physics, the isolated large pores (green part in Fig. 2b) are treated as another solid phase without contribution to the gas diffusion path in the simulation.

2.2 Governing Equation and Numerical Methods

2.2.1 Governing Equation

The gas diffusion process is driven by the gradient of chemical potential which is dependent on the gas concentration, temperature and pressure (Bird et al. 2002). In this work, we consider the binary gas diffusion through three-dimensional porous structures with the following assumptions (He et al. 2017): (1) the system is in dynamic equilibrium state where advection is negligible; (2) steady-state diffusion is considered; (3) the temperature and total pressure of the system remains constant; (4) the gas concentration is low. When the pore size is much larger than the gas MFP, the diffusion process is well described by the Fick’s second law:

$$\nabla \cdot (D_b \nabla C) = 0, \tag{3}$$

where C is the gas concentration and D_b is the bulk binary gas diffusivity. For gas diffusion in nanoporous structures in the present study, the average pore size is at the order of one hundred nanometers, which is comparable to the gas MFP around ambient pressure and temperature. The Fick’s law of diffusion is in principle no longer valid for this situation where Knudsen diffusion plays an appreciable role. Inspired from the modeling of microscale and nanoscale gas flow by Navier–Stokes equation with a size-dependent effective viscosity (Beskok and Karniadakis 1999; Wang et al. 2016), we propose to model the gas diffusion in nanoporous structures by Eq. (3) with a local diffusion coefficient:

$$\nabla \cdot (D_{\text{pore}} \nabla C) = 0, \tag{4}$$

where D_{pore} denotes the local diffusion coefficient dependent on the ratio of gas MFP to local pore size (exactly the local Knudsen number).

Concentration boundary conditions are specified for Eq. (4):

$$\begin{cases} C = C_{\text{in}}, & x = 0 \\ C = C_{\text{out}}, & x = L \end{cases}, \tag{5}$$

where L is the length of the computational domain with an inlet and an outlet keeping at a constant gas concentration C_{in} and C_{out} , respectively. The lateral boundaries of the computational domain are assumed periodic.

2.2.2 Local Diffusion Coefficient

The determination of local diffusion coefficient in Eq. (4) is crucial for accurate modeling of gas diffusion in the transition regime where the gas MFP is comparable to the characteristic length. It is very difficult to analytically obtain a solution to the Boltzmann transport equation (BTE) in the transition regime, which often has to recourse to numerical schemes such as the DSMC method. The empirical Bosanquet formula has been proposed in the previous work to calculate the gas diffusivity in the transition regime (Pollard and Present 1948; Krishna and van Baten 2012):

$$\frac{1}{D_{pore}} = \frac{1}{D_b} + \frac{1}{D_K}, \tag{6}$$

where D_b and D_K represent the gas molecular diffusivity and Knudsen diffusivity, respectively. The microscopic expression of molecular diffusivity is derived through a Chapman–Enskog expansion solution to BTE (Blundell and Blundell 2009; Chapman and Cowling 1953):

$$D_b = \frac{3k_B T}{8\rho d_g^2} \sqrt{\frac{k_B T}{\pi m}} = \frac{3\pi}{16} \lambda \bar{c} \approx \frac{3}{5} \lambda \bar{c}, \tag{7}$$

with the gas MFP $\lambda = k_B T / (p\sqrt{2\pi}d_g^2)$ and mean molecular velocity $\bar{c} = \sqrt{8k_B T / \pi m}$, k_B , d_g and m being the Boltzmann constant, molecular diameter and mass, respectively. Equation (7) is valid whenever the gas can be treated as idea gas (Chapman and Cowling 1953). The Knudsen diffusivity has also been derived in the kinetic theory of gas (Bird et al. 2002; Kärger et al. 2012):

$$D_K = \frac{4d}{3} \sqrt{\frac{k_B T}{2\pi m}} = \frac{1}{3} d \bar{c}, \tag{8}$$

where d is the local pore size. Substitution of Eqs. (7) and (8) into Eq. (6) results in the following relation:

$$\frac{D_{pore}}{D_b} = \frac{1}{1 + \frac{9}{5} Kn}, \tag{9}$$

where the Knudsen number is defined as: $Kn = \lambda/d$. In some other work, the molecular diffusivity from a simple kinetic theory formula instead of Eq. (7) is adopted (Blundell and Blundell 2009): $D_b = \frac{1}{3} \lambda \bar{c}$, which gives rise to the following relation (Berson et al. 2011; Pollard and Present 1948):

$$\frac{D_{pore}}{D_b} = \frac{1}{1 + Kn}. \tag{10}$$

Thus, we provide the following corrected Bosanquet-type formula from Eqs. (9) and (10) to describe the gas diffusion in transition regime:

$$\frac{D_{pore}}{D_b} = \frac{1}{1 + \alpha Kn}, \tag{11}$$

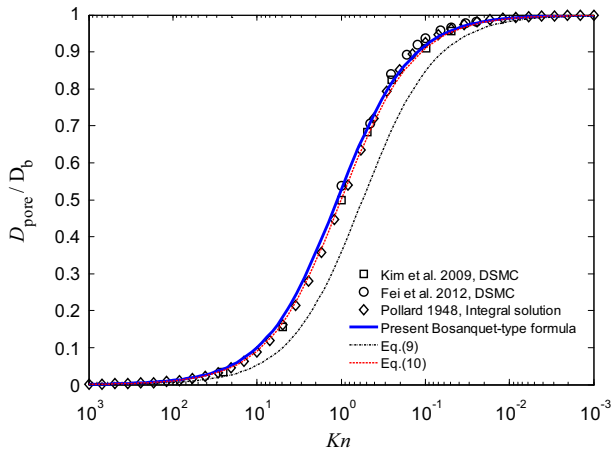


Fig. 3 Local diffusion coefficient versus Knudsen number: the squares and circles represent the DSMC (Direct Simulation Monte Carlo) results from Ref. Kim et al. (2009) and Fei et al. (2012), respectively, the diamonds denote the integral solution of Boltzmann transport equation (Pollard and Present 1948), whereas the solid line denotes the present corrected Bosanquet-type formula: $D_{\text{pore}}/D_b = 1/(1 + 0.9 Kn)$, with the Knudsen number defined as the ratio of gas mean free path to local pore diameter, the dashed-dotted line and the dashed line denote, respectively, Eqs. (9) and (10) from the original Bosanquet formula

where the empirical coefficient α is determined through fitting the solution of the BTE for gas diffusion in straight channel. We find that Eq. (11) with $\alpha = 0.9$ predicts the gas diffusion coefficient in overall good agreement with the DSMC and the integral solutions of BTE in the whole range of transport regimes, as shown in Fig. 3. In comparison with the previous determination of local diffusion coefficient based on the original Bosanquet formula Eq. (6) without solid verification (Lange et al. 2011; Chen et al. 2015; Siddique and Liu 2010), we adopt a calibrated one to accurately describe the gas diffusion within the transition from molecular diffusion regime to Knudsen diffusion regime. Equation (9) derived from Eq. (6) much underestimates the local diffusion coefficient as shown in Fig. 3. Although Eq. (10) has a comparable performance to Eq. (11) with $\alpha = 0.9$, the latter is adopted in the present work as the coefficient $\alpha = 0.9$ is specified by best fitting process with least standard deviation for all data points of BTE solution.

2.2.3 Determination of Local Knudsen Number

The calculation of the local diffusion coefficient in Eq. (11) requires the value of local Knudsen number as the ratio of gas MFP to local pore size. There are mainly two methods for computing the local pore diameter throughout the porous structure: (1) largest sphere method (Delerue et al. 1999; Bhattacharya and Gubbins 2006) and (2) 13-length averaging method (Lange et al. 2010). We choose the largest sphere method in this work due to the following two points: (1) the physical picture of largest sphere method is very close to that of the interaction between gas molecules and solid wall in Knudsen diffusion; (2) the 13-length averaging method will much overestimate the pore diameter of the slender pores with a large length/width ratio. The main idea of the largest sphere method is to find the diameter of the largest sphere that can be fitted inside a pore at a given point in the porous structure (Bhattacharya and Gubbins 2006). The procedures in implementing the largest sphere method are given as follows (Bhattacharya and Gubbins 2006): (1) calculate the distances of any point

X in the pore from all the points in solid phase of the porous media, which form a set of distances $\{d_X\}$; (2) choose the minimum element in the set $\{d_X\}$ for each point X as the radius of sphere centered on the point X, and the spheres for all the points in the pore form a set of spheres $\{P\}$; (3) for any point X' in the pore, choose the largest sphere in the set $\{P\}$ that contains the point X' , and the diameter of this sphere is specified as the pore size of the point X' . Besides the shape resistance from the solid phase (including the isolated pore) of porous media which has no contribution to diffusion path, the local pore geometry introduces an additional transport resistance through Eq. (11) due to the gas-wall interaction from Knudsen diffusion.

2.2.4 MRT Lattice Boltzmann Method

In contrast to the SRT-LBM for solution of Eq. (3) for Fickian gas diffusion in porous structures (He et al. 2017), the MRT-LBM (Yoshida and Nagaoka 2010) is used to solve Eq. (4) for gas diffusion in nanoporous structures. It has been shown in a recent study that the predicted effective diffusivity in simple porous media composed of cylinders in a square or staggered arrangement based on the SRT-LBM is dependent on the relaxation time, which is an artifact and can be eliminated in the MRT-LBM (Chai et al. 2016). Because of the position dependent non-dimensional relaxation time in Eq. (16), the MRT-LBM is a better choice for modeling gas Knudsen diffusion in nanoporous structures. The lattice evolution equation in MRT-LBM is:

$$g_\alpha(\mathbf{r} + \mathbf{e}_\alpha \delta_t, t + \delta_t) - g_\alpha(\mathbf{r}, t) = - \sum_\beta (\mathbf{M}^{-1} \mathbf{S} \mathbf{M})_{\alpha\beta} [g_\beta(\mathbf{r}, t) - g_\beta^{\text{eq}}(\mathbf{r}, t)], \tag{12}$$

where $g_\alpha^{\text{eq}}(\mathbf{r}, t)$ is the local equilibrium distribution function at position \mathbf{r} and time t for the lattice direction α , with \mathbf{e}_α being the discrete lattice velocities in D3Q7 lattice system used in this work. \mathbf{M} is the matrix that projects a vector onto the moment space, whereas \mathbf{S} is the relaxation-time matrix. The local equilibrium distribution function is related to the gas concentration C as:

$$g_\alpha^{\text{eq}} = \begin{cases} \frac{C}{4}, & \alpha = 0 \\ \frac{C}{8}, & \alpha = 1 - 6 \end{cases}. \tag{13}$$

The discrete lattice velocities are expressed as:

$$\mathbf{e}_\alpha = \begin{cases} (0, 0, 0)c, & \alpha = 0 \\ (\pm 1, 0, 0)c, (0, \pm 1, 0)c, (0, 0, \pm 1)c, & \alpha = 1 - 6 \end{cases}, \tag{14}$$

where c is the lattice speed. The matrices \mathbf{M} and \mathbf{S} have been, respectively, constructed as (Yoshida and Nagaoka 2010):

$$\mathbf{M} = \begin{pmatrix} 1 & 1 & 1 & 1 & 1 & 1 & 1 \\ 0 & 1 & -1 & 0 & 0 & 0 & 0 \\ 0 & 0 & 0 & 1 & -1 & 0 & 0 \\ 0 & 0 & 0 & 0 & 0 & 1 & -1 \\ 6 & -1 & -1 & -1 & -1 & -1 & -1 \\ 0 & 2 & 2 & -1 & -1 & -1 & -1 \\ 0 & 0 & 0 & 1 & 1 & -1 & -1 \end{pmatrix}, \quad \mathbf{S} = \begin{pmatrix} \tau_0 & 0 & 0 & 0 & 0 & 0 & 0 \\ 0 & \tau_{xx} & \tau_{xy} & \tau_{xz} & 0 & 0 & 0 \\ 0 & \tau_{xy} & \tau_{yy} & \tau_{yz} & 0 & 0 & 0 \\ 0 & \tau_{xz} & \tau_{yz} & \tau_{zz} & 0 & 0 & 0 \\ 0 & 0 & 0 & 0 & \tau_4 & 0 & 0 \\ 0 & 0 & 0 & 0 & 0 & \tau_5 & 0 \\ 0 & 0 & 0 & 0 & 0 & 0 & \tau_6 \end{pmatrix}, \tag{15}$$

where the relaxation times are $\tau_0 = \tau_4 = \tau_5 = \tau_6 = 1$ and:

$$\tau_{ij} = \left(\frac{1}{2} + \frac{4D_{pore}}{c^2 \delta_t} \right) \delta_{ij} \quad (i, j = x, y, z), \tag{16}$$

with δ_{ij} denoting the Kronecker symbol.

After the solution of local distribution function is obtained, the macroscopic variables including the gas concentration C and mass flux \mathbf{J} are computed through statistical process:

$$C = \sum_{\alpha} g_{\alpha}, \tag{17}$$

$$\mathbf{J} = \frac{\tau_{ii} - 0.5}{\tau_{ii}} \sum_{\alpha} g_{\alpha} \mathbf{e}_{\alpha}, \tag{18}$$

with $\tau_{ii} = \tau_{xx} = \tau_{yy} = \tau_{zz}$ as we consider isotropic local gas diffusion coefficient. Once the gas Knudsen diffusion is resolved, the overall effective gas diffusion coefficient of the nanoporous structure is calculated based on the Fick's law:

$$D_{\text{eff, Kn}} = \frac{L \int J dA}{\Delta C \int dA}, \tag{19}$$

where the gas concentration difference is $\Delta C = C_{\text{in}} - C_{\text{out}}$, and J is the component of \mathbf{J} along the overall transport direction.

The boundary treatment in the MRT-LBM is the same as that in the SRT-LBM for diffusion in porous structure (He et al. 2017). The standard bounce-back scheme is used for the solid wall around the pore inside the structure, and the non-equilibrium bounce-back scheme is adopted for the concentration boundary at the inlet and outlet. After an independence check, a grid of $80 \times 80 \times 80$ is adopted for the computational domain throughout the present work except the diffusion in layering structures due to the structure compression in one direction in Sect. 4.4. Such a domain size and grid resolution is sufficient to satisfy the REV requirement as is demonstrated extensively in our previous studies (Wang and Pan 2008; He et al. 2017; Wang 2012). In addition, the exact morphology for the reconstructed porous structure based on the same statistical parameters has been shown to have negligible effect on the results of effective gas diffusion coefficient.

3 Validations

In this section, the numerical framework including the structure reconstruction algorithm and MRT-LBM in Sect. 2 will be validated by modeling gas Knudsen diffusion in MPL and CL nanoporous materials, respectively.

3.1 Comparison to Experiment on Gas Diffusion in Microporous Layer

Firstly, we consider gas diffusion in MPL structure. We apply the reconstruction algorithm to generate the digital MPL structure, which is then introduced into the MRT-LBM model to compute the effective gas diffusivity. The structure porosity in the present simulation is consistent with that in the experiment. In terms of the seed distribution probability used in generating the granular MPL, we adopt a typical value of $s_d = 0.01$ from Ref. Wang et al. (2007) after verifying that the numerical results are insensitive to its value. The details of the directional growth probability matrix D_i can be also found in Ref. Wang et al. (2007). The lattice step is determined by equalizing the average pore diameter in lattice units of the reconstructed MPL to the measured average pore diameter of MPL. The average pore diameter of the reconstructed MPL is calculated as a probabilistic average of the local pore diameter distribution obtained by the largest sphere method. The gas MFP is calculated based

Table 1 Effective diffusion coefficient of oxygen in MPL structure with a porosity 0.64 and an average pore diameter 24 nm at $p=94\text{--}97$ kPa, $t=22$ °C

Effective gas diffusion coefficient	$D_{\text{eff}} \times 10^6 \text{m}^2/\text{s}$	$D_{\text{eff}}/D_{\text{b}}$
Experimental (Chan et al. 2012)	1.50 ± 0.2	0.0701 ± 0.0093
Present prediction by LBM	1.77	0.0827
Bruggeman's formula (Bruggeman 1935)	10.96	0.5120

on the formula: $\lambda = k_{\text{B}}T / \left(p\sqrt{2}\pi d_{\text{g}}^2 \right)$, with the molecular diameter for oxygen molecule $d_{\text{g}} = 3.6 \times 10^{-10}$ m (Haynes et al. 2012). The gas bulk diffusivity [cm^2/s] is calculated based on the following empirical relation (Chan et al. 2012):

$$\ln(p \cdot D_{\text{b}}) = \ln(1.13 \times 10^{-5}) + 1.724 \ln(T), \quad (20)$$

where p is the total gas pressure [atm] and T is the thermodynamic temperature [K]. After the gas concentration and mass flux are obtained through a statistical summation of the discrete distribution function based on Eqs. (17) and (18), the effective gas diffusivity of the porous structure is computed through integrating the local mass flux along an arbitrary cross-section perpendicular to the overall transport direction based on Eq. (19).

We compare the present predictions to two room-temperature experimental results of oxygen diffusion in MPL structures at 1 atm pressure (Chan et al. 2012) and at 2 atm pressure (Inoue et al. 2016) in Table 1 and in Fig. 4, respectively. The globally good agreement between the numerical prediction and the experimental data demonstrates the capability of the new computational framework. The minor deviation between them may be attributed to the fact that the average pore diameter rather than the exact pore size distribution in the simulation has been set the same as that in the experiment. In Table 1, we also include the result from the Bruggeman's empirical formula (Bruggeman 1935): $D_{\text{eff}}/D_{\text{b}} = \varepsilon^{1.5}$, which much overestimates the actual effective gas diffusion coefficient because of neglecting the effect of Knudsen diffusion and an oversimplification of the diffusion process.

3.2 Comparison to Experiment on Gas Diffusion in Catalyst Layer

In this subsection, we consider the gas diffusion in CL structure. The numerical methodology is the same as that for MPL structure in Sect. 3.1 except a further generation of isolated large pores in the porous material. The present LBM simulation predicts the effective gas diffusion coefficient in good agreement with the results by experimental measurement in CL materials (Inoue et al. 2016; Yu and Carter 2010; Yu et al. 2012), as shown in Fig. 5a, b. We also include in Fig. 5a the results in several previous numerical studies on the same gas diffusion process by FVM (Lange et al. 2012; Siddique and Liu 2010) and LBM (Chen et al. 2015) solution of the diffusion equation. It is seen that the present prediction is the closest one to the experimental result. The improvement of the present numerical framework over the previous ones is mainly attributed to the following four aspects: (1) the significant morphology feature of 'isolated large pore' in CL structure carefully considered here was not taken into account in previous work (Lange et al. 2012; Chen et al. 2015; Siddique and Liu 2010); (2) the more accurate and robust MRT-LBM is used in contrast to the SRT-LBM in previous work (Chen et al. 2015); (3) the corrected Bosanquet-type formula Eq. (11) is adopted to determine

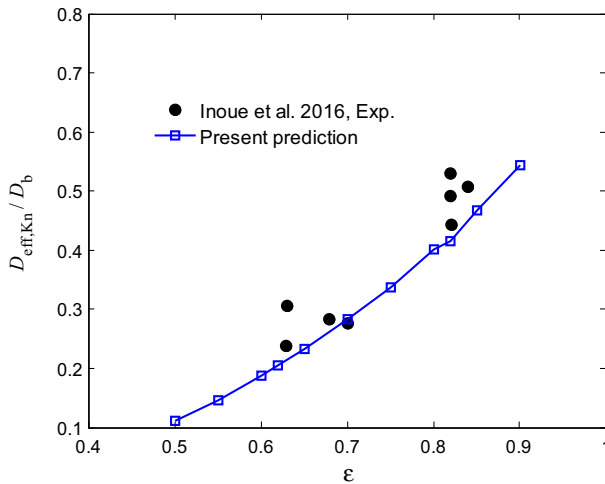


Fig. 4 Non-dimensional effective gas diffusion coefficient of microporous layer (MPL) structure: the filled circles represent the results from experimental measurement of oxygen diffusion with $D_b = 0.1 \times 10^{-4} \text{ m}^2/\text{s}$ in MPL with an average pore diameter 80 nm at a pressure $p = 201 \text{ kPa}$ and temperature $t = 22 \text{ }^\circ\text{C}$ (Inoue et al. 2016), whereas the square-line represents the prediction by the present LBM simulation

the local diffusion coefficient in contrast to the original Bosanquet formula Eq. (6) in the previous work (Lange et al. 2012; Chen et al. 2015; Siddique and Liu 2010); (4) the largest sphere method used in the present work is more appropriate than the 13-length averaging method (Lange et al. 2012; Chen et al. 2015) as explained in Sect. 2.2.3. Therefore, it is crucial to capture both the pore-scale structures and the local diffusion coefficient in order to accurately model the gas Knudsen diffusion in CL structure. The good agreement between the present numerical prediction and the experimental result also indicates the power of pore-scale simulation. The influence of the very special morphology ‘isolated large pore’ on transport properties of CL structure is significant, which is very difficult to be well captured by an effective model at the Darcy scale. The power of pore-scale simulation is to recover the macroscopic transport behaviors in porous medium through resolving the microscopic details of pore structures. Since the CL structure has nearly the same backbone as the MPL structure, the effect of ‘isolated large pore’ can be estimated by comparing the effective gas diffusivity of the former to that of the latter with a porosity equal to the background porosity (ϵ_{micro}) of the former. On the other hand, the contribution of Knudsen diffusion can be roughly separated by comparing the present numerical result to that of a LBM simulation of Fickian diffusion through the same structure yet without using the Bosanquet-type formula and largest sphere method to determine the local diffusion coefficient.

4 Numerical Results and Discussions

In this section, the validated numerical framework will be used to study various important influencing factors on the effective gas diffusion coefficient of nanoporous materials including the morphology effect of isotropic microstructure in Sect. 4.1, the size effect in Sect. 4.2, the anisotropic effect of microstructure in Sect. 4.3 and the layering structure effect in Sect. 4.4. Furthermore, we find a surprisingly widely applicable relation between the normalized effec-

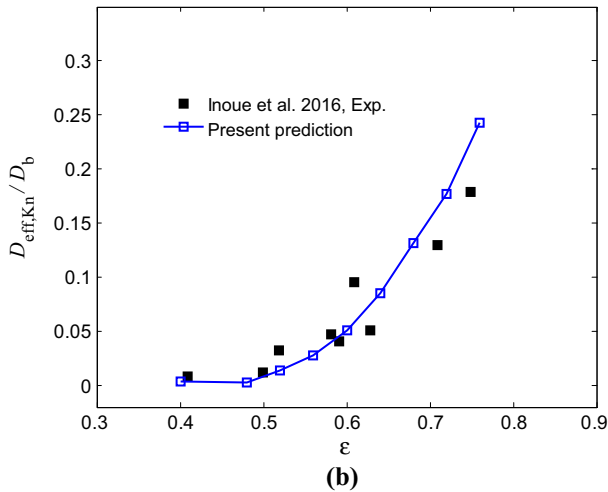
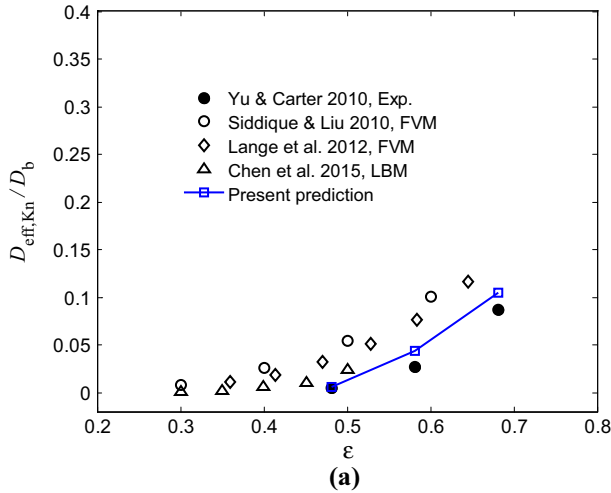


Fig. 5 Non-dimensional effective gas diffusion coefficient of catalyst layer (CL) structure: **a** the filled circles denote the results from experimental measurement of oxygen with $D_b = 0.27 \text{ cm}^2/\text{s}$ in CL with average pore diameter 36 nm, 60 nm and 100 nm, respectively, at $p = 101 \text{ kPa}$, $t = 80^\circ \text{C}$ (Yu and Carter 2010; Yu et al. 2012), the circles and diamonds denote the predictions by FVM simulation in Refs. Siddique and Liu (2010) and Lange et al. (2012), respectively, the triangles denote the prediction by LBM simulation in Ref. Chen et al. (2015), the square-line represents the present prediction by LBM simulation considering the isolated large pore; **b** the filled squares denote the results from experimental measurement of oxygen with $D_b = 0.1 \text{ cm}^2/\text{s}$ in CL with average pore diameter 60 nm at $p = 201 \text{ kPa}$, $t = 22^\circ \text{C}$ (Inoue et al. 2016), the square-line represents the present prediction by LBM simulation considering the isolated large pore. The ratio of isolated large pore is related to the porosity through the empirical linear expression: $R = a\varepsilon_{\text{density}} + b$, with $a = -1.7658$ and $b = 1.4443$

tive gas diffusion coefficient by the corresponding effective Fickian diffusion coefficient and the average Knudsen number:

$$\frac{D_{\text{eff, Kn}}}{D_{\text{eff, Fick}}} = \frac{1}{1 + 0.9 \langle Kn \rangle}, \quad (21)$$

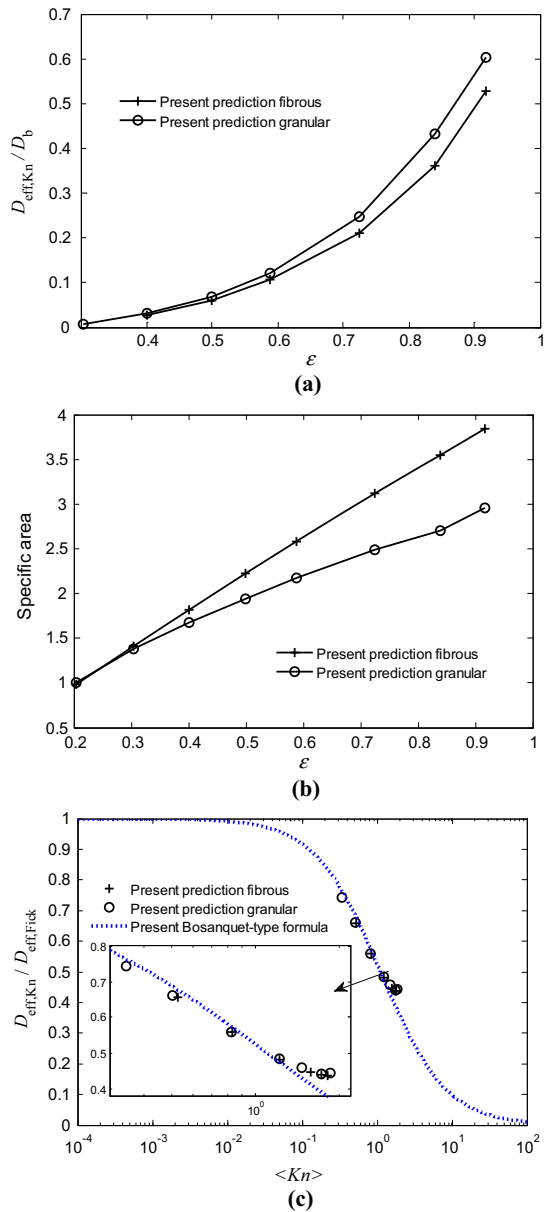
where the average Knudsen number $\langle Kn \rangle$ is defined as the ratio of gas MFP to the average pore diameter of the nanoporous structure. Although the present numerical framework is powerful for gas diffusion in any kinds of nanoporous materials, the pore-scale simulation is often computationally intensive and time-consuming. Thus, an effective analytical model Eq. (21) at the Darcy scale extracted from our simulation will be very helpful for a convenient estimation of effective gas diffusivity of many nanoporous structures in the future.

4.1 Morphology Effect of Isotropic Microstructure

The microscopic morphology of porous structures has been demonstrated to have significant influence on the effective transport properties, such as the electrical and thermal conductivities (Wang and Pan 2008), and the fluid flow permeability (Wang 2012; Cousins et al. 2018). We also study the morphology effect on gas Fickian diffusion in porous media in our recent work (He et al. 2017), where the fibrous and granular porous structures are found to have nearly the same effective diffusion coefficient at the same porosity. However, it was anticipated that the morphology will impact the gas diffusion coefficient when surface-dependent physical–chemical processes take place because of the large difference of specific surface area found between fibrous and granular porous media (He et al. 2017). Since gas–surface interaction plays an important role in gas Knudsen diffusion through the nanoporous material, we consider the morphology effect again. For a consistent comparison on the same ground, the isotropic fibrous and granular porous structures are taken into account. The numerical reconstruction of the fibrous porous structures can be found in our previous work (He et al. 2017). The seed distribution probability of granular porous structure is set the same as that of fibrous porous structure with the same porosity. The lattice step is set as 20 nm in the simulation such that the dimension of computational domain is $1.6 \mu\text{m} \times 1.6 \mu\text{m} \times 1.6 \mu\text{m}$. The predicted effective gas diffusion coefficients of fibrous and granular porous structures are shown in Fig. 6a, where an appreciable difference is found between them especially at high porosities. The difference is attributed to the larger specific surface area of fibrous structure than granular structure seen in Fig. 6b, which results in stronger gas diffusion resistance from surface confinement and thus lower effective diffusion coefficient. Once normalized by the corresponding Fickian counterpart (He et al. 2017), the effective gas diffusion coefficient of the two porous structures with different morphology can be well fitted into a single relation Eq. (21), as shown in Fig. 6c.

Although there is minor deviation of the numerical results from the prediction by Eq. (21) at low porosity, the latter displays a globally good performance. This unified relation Eq. (21) can be used for a fast estimation of the effective diffusion coefficient of a nanoporous material through the following simple steps: (1) get the effective Fickian diffusion coefficient of similar porous media with the same porosity from the existing fruitful experimental data or empirical relation (Zamel and Li 2013; He et al. 2017; Ismail et al. 2015); (2) get the average pore diameter of this nanoporous material by MIP or nitrogen adsorption methods and determine the average Knudsen number.

Fig. 6 Morphology effect on effective gas diffusion coefficient in isotropic fibrous and granular porous structures: **a** effective gas diffusion coefficient normalized by bulk diffusion coefficient versus porosity, the circle-line and cross-line denote the present prediction by LBM simulation for granular and fibrous porous structures, respectively, with lattice step 20 nm at $p=1$ atm, $t=20$ °C, with $D_b = 0.22$ cm²/s; **b** specific area of granular and fibrous porous structures, respectively, the legend is the same as that in **a**; **c** effective gas diffusion coefficient normalized by effective Fickian diffusion coefficient versus average Knudsen number $\langle Kn \rangle$, the circles and cross symbols represent the present results of fibrous and granular structures, respectively, whereas the dotted line represents the present Bosanquet-type empirical formula: $D_{\text{eff},Kn}/D_{\text{eff},Fick} = 1/(1 + 0.9 \langle Kn \rangle)$, where $\langle Kn \rangle$ is defined as the ratio of gas mean free path to the average pore diameter obtained by largest sphere method, the inset figure demonstrates the minor deviation of the simulation results from the empirical formula at low porosity



4.2 Size Effect

The gas Knudsen diffusion in a nanoporous material is much influenced by the average Knudsen number as the ratio of gas MFP to average pore size. The gas MFP of a certain gas is dependent on the pressure and temperature as $\lambda = k_B T / (p \sqrt{2} \pi d_g^2)$. In actual engineering applications such as in the fuel cell (FC), the operating conditions (mainly including temperature and pressure) may change a lot; on the other hand, the electrode

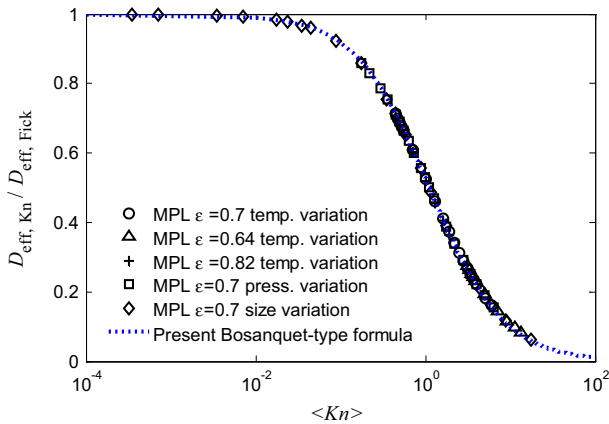


Fig. 7 Size effect on non-dimensional effective gas diffusion coefficient of MPL structure: the circles represent the MPL structure with porosity $\varepsilon = 0.7$ and average pore diameter 80 nm at $p = 2$ atm taken from Ref. Inoue et al. (2016), the triangles represent the MPL structure with porosity $\varepsilon = 0.64$ and average pore diameter 24 nm at $p = 1$ atm taken from Ref. Chan et al. (2012), the cross symbols represent the MPL structure with porosity $\varepsilon = 0.82$ and average pore diameter 80 nm at $p = 2$ atm taken from Ref. (Inoue et al. 2016), the temperature varies within the scope 22–3800 °C for the circles, triangles and cross symbols; the squares represent the MPL structure with porosity $\varepsilon = 0.7$ and average pore diameter 80 nm at $t = 22$ °C taken from Ref. (Inoue et al. 2016), the pressure varies within the scope 14–500 kPa; the diamonds represent the MPL structure with porosity $\varepsilon = 0.7$ at $p = 2$ atm, $t = 22$ °C taken from Ref. Inoue et al. (2016), the average pore diameter varies within the scope 2– 10^5 nm. The dotted line represents the present Bosanquet-type empirical formula: $D_{\text{eff,Kn}}/D_{\text{eff,Fick}} = 1/(1 + 0.9 \langle Kn \rangle)$, where $\langle Kn \rangle$ is defined as the ratio of gas mean free path to the average pore diameter obtained by largest sphere method

structures in different categories of FCs may have different pore size distributions and average pore diameters (Yuan and Sundén 2014). Therefore, it is crucial to evaluate the effective gas diffusion coefficient of a nanoporous structure with various average pore sizes under various system temperatures and pressures. To obtain meaningful results, we take the actual MPL structures with porosities 0.64, 0.7 and 0.82, respectively, from two previous experimental studies (Inoue et al. 2016; Chan et al. 2012). The influences of temperature, pressure and pore size are studied separately by varying one parameter while keeping the other two invariable. The gas diffusions in all the three MPL structures are simulated when studying the temperature effect within a scope 22–3800 °C, whereas gas diffusion in the MPL structure with porosity 0.7 is merely simulated when studying the pressure effect within a scope 14–500 kPa and the average pore size effect within a scope 2– 10^5 nm due to the similarity. The considered parameter scope of temperature, pressure and pore size is sufficient to cover the possible range of values in actual application (Yuan and Sundén 2014).

The predicted effective gas diffusivity at various temperatures, pressures and pore sizes is shown in Fig. 7. It is surprisingly found that the Bosanquet-type empirical formula Eq. (21) provides a perfect description of the reduction of normalized effective gas diffusion coefficient due to the increase in average Knudsen number from increasing temperature, decreasing pressure or average pore size. Therefore, Eq. (21) can be used for an estimation of the effective gas diffusivity of nanoporous materials under in situ operating condition with the help of test results at specific temperature and pressure.

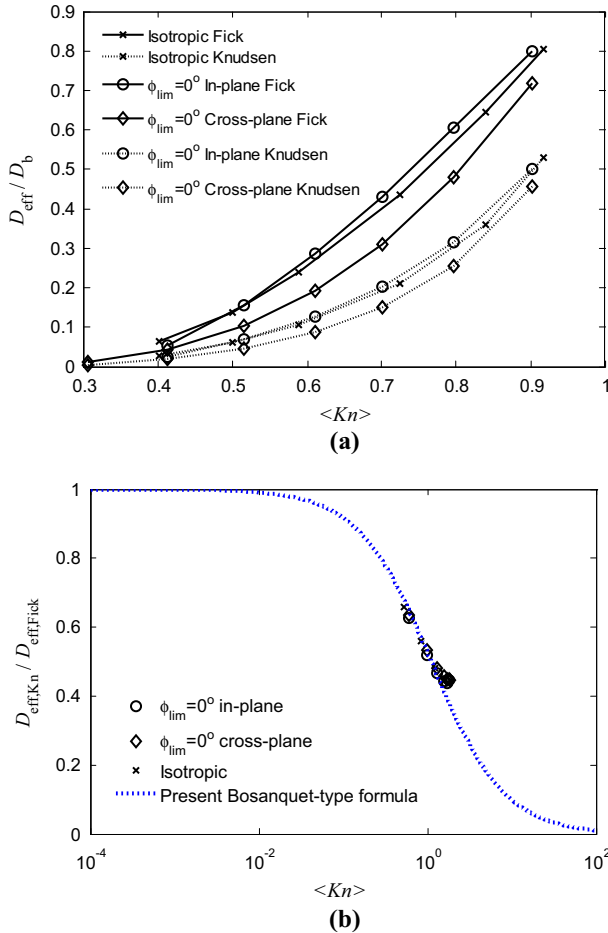


Fig. 8 Anisotropic effective gas diffusion coefficient in fibrous structures: **a** effective gas diffusion coefficient normalized by bulk diffusion coefficient versus average Knudsen number, the solid lines with symbols represent the results of Fickian diffusion in isotropic structure, in-plane and cross-plane Fickian diffusion in anisotropic fibrous structure with $\phi_{lim} = 0^\circ$, $\theta_{lim} = 180^\circ$ (isotropic in the in-plane direction) at $p=1$ atm, $t=22$ °C with $D_b = 0.214$ cm²/s, whereas the dotted lines with symbols represent the results of Knudsen diffusion in the same structures, respectively, a lattice step 20 nm is adopted in the LBM simulation; **b** effective gas Knudsen diffusion coefficient normalized by effective Fickian diffusion coefficient, the symbols denote the present predictions by LBM simulation, whereas the dotted line denotes the present Bosanquet-type empirical formula: $D_{eff,Kn}/D_{eff,Fick} = 1/(1+0.9\langle Kn \rangle)$, where $\langle Kn \rangle$ is defined as the ratio of gas mean free path to the average pore diameter obtained by largest sphere method

4.3 Anisotropy Effect of Microstructure

The fibrous material often becomes anisotropic during the manufacturing process or just required by actual application. The anisotropy of fibrous material is featured by the limits of two geometrical orientation angles (ϕ_{lim} , θ_{lim}) (Wang and Pan 2008; He et al. 2017; Wang et al. 2007). The effective gas diffusion coefficient along the fiber’s direction is larger than that across the fiber’s direction, defined as the in-plane and cross-plane diffusion coefficients, respectively. Thus, the difference between the in-plane and cross-plane effective gas diffusion

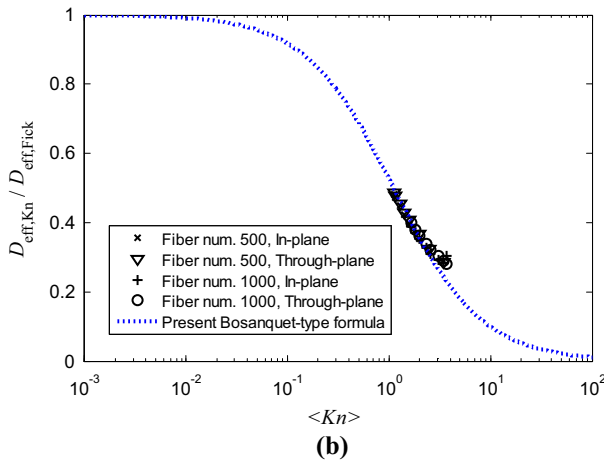
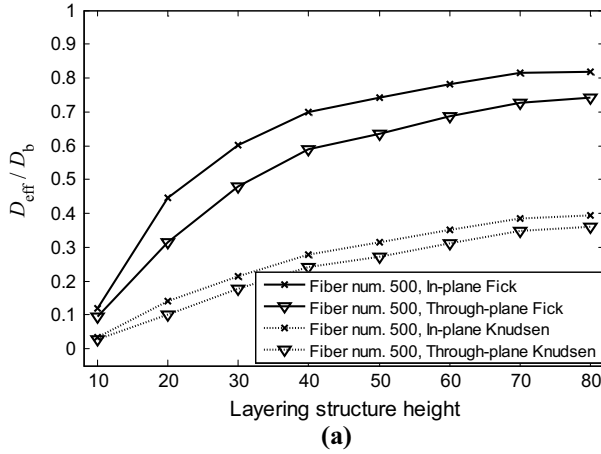


Fig. 9 Effective gas diffusion coefficient in layering structures with specified fiber numbers: **a** effective gas diffusion coefficient normalized by bulk diffusion coefficient versus layering structure height in lattice units, the solid lines with symbols represent the results of in-plane and through-plane Fickian diffusion in layering structure with 500 fibers, whereas the dotted lines with symbols represent the results of in-plane and through-plane Knudsen diffusion in the same structure; **b** effective gas Knudsen diffusion coefficient normalized by effective Fickian diffusion coefficient versus average Knudsen number, the symbols denote the present results for layering structures with 500 and 1000 fibers, respectively, whereas the dotted line denotes the present Bosanquet-type empirical formula: $D_{\text{eff,Kn}}/D_{\text{eff,Fick}} = 1/(1 + 0.9\langle Kn \rangle)$, where $\langle Kn \rangle$ is defined as the ratio of gas mean free path to the average pore diameter obtained by largest sphere method. A lattice step 10 nm is adopted in the LBM simulation at $p=1$ atm, $t=22$ °C with $D_b = 0.214$ cm²/s

coefficients is used to characterize the anisotropy effect of microstructure. In our previous study (He et al. 2017), the influence of orientation angle ϕ_{lim} on the effective Fickian diffusion coefficient is systematically investigated, with an empirical correlation provided through fitting a series of simulation results. Here, we explore the anisotropy effect on gas Knudsen diffusion in nanoporous fibrous material. The lattice step is set as 20 nm in the simulation such that the dimension of computational domain is $1.6 \mu\text{m} \times 1.6 \mu\text{m} \times 1.6 \mu\text{m}$. The effective gas diffusion coefficients along both in-plane and cross-plane directions of the anisotropic fibrous material with typical orientation angles $\phi_{\text{lim}} = 0^\circ$, $\theta_{\text{lim}} = 180^\circ$ and the results for the isotropic

structure are shown in Fig. 8a, where the results of Fickian diffusion are also included for a comparison. Although the effective gas Knudsen diffusion coefficients are reduced as a whole compared to the Fickian counterpart, there still exists difference between the result along in-plane direction and that along cross-plane direction. Fortunately, after normalization by the corresponding Fickian result, as seen in Fig. 8b, the effective gas diffusion coefficient along both in-plane and cross-plane direction can be well described by the empirical relation Eq. (21). As a benefit, the effective gas diffusivity of nanoporous fibrous materials with other orientation angles can be determined with the help of this unified relation and the obtained empirical correlation for the Fickian counterpart in our previous study (He et al. 2017).

4.4 Layering Structures Effect

The fibrous gas diffusion layer (GDL) or non-woven layer may be compressed during the application process (Froning et al. 2013; Froning et al. 2016). The effective gas diffusion coefficient will be thus affected due to the change of structure porosity and average pore size under compression. In this work, we reconstruct the layering fibrous structures with $\phi_{\text{lim}} = 0^\circ$, $\theta_{\text{lim}} = 180^\circ$ and fixed fiber number of 500 and 1000, respectively. A grid of 80×80 is adopted for the length and width directions of the computational domain, whereas various grids from 10 to 80 are used for the height direction to represent different layering structure heights under compression. The lattice step is set as 10 nm, such that the length and width of the computational domain are $800 \text{ nm} \times 800 \text{ nm}$ and the height varies from 100 to 800 nm. The effective gas diffusion coefficient for the case of 500 fibers is displayed in Fig. 9a and is found to decrease with decreasing the layering structure height. The increase in gas diffusion resistance under compression is mainly caused by the dimension reduction and porosity drop of the structure. Furthermore, the reduction in effective gas Knudsen diffusivity is found almost twice of the reduction in the Fickian counterpart when the layering structure height varies from 80 to 10 lattice units. This strong reduction in nanoporous material comes from the enhancement of Knudsen diffusion due to decreasing average pore diameter under compression. Finally, the empirical Bosanquet-type formula Eq. (21) demonstrates a good performance in describing the normalized effective gas diffusion coefficient of layering structure as well.

5 Conclusions

We develop an efficient computational framework to model gas diffusion through nanoporous materials including a structure reconstruction algorithm and a MRT lattice Boltzmann method. Through a comprehensive study of the microstructure effects on effective gas diffusion coefficient, we obtain the following conclusions:

1. Different morphologies of nanoporous materials will give rise to different effective diffusivity in gas Knudsen diffusion because of different system specific surface areas. A larger system specific surface area will result in the stronger gas diffusion resistance from surface confinement. Thus, the effective gas diffusion coefficient of granular nanoporous material is found to be higher than that of fibrous nanoporous material with the same porosity;
2. The effective gas diffusion coefficient of nanoporous material will decrease with increasing the system temperature or decreasing the gas total pressure and average pore size, all of which render an increase of average Knudsen number;

3. The fiber orientation in fibrous nanoporous material will cause anisotropic effective gas diffusivity, with the diffusion resistance along the fiber direction smaller than that across the fiber direction. For layering structures with fixed number of fibers, a decreasing structure height caused by compression will result in a reduction of effective gas diffusion coefficient, with the reduction times in gas Knudsen diffusion much higher than that in Fickian diffusion;
4. A widely applicable relation is found between the normalized effective gas diffusion coefficient of nanoporous material and the average Knudsen number in spite of different microstructures. This unified relation will provide a fast estimation of effective gas diffusivity of nanoporous materials in engineering application.

Acknowledgements The authors appreciate helpful discussions with Prof. N. Pan. This work is financially supported by the NSF grant of China (No. U1562217) and the National Science and Technology Major Project on Oil and Gas (No. 2017ZX05013001).

References

- Andisheh-Tadmir, M., El Hannach, M., Kjeang, E., Bahrami, M.: An analytical relationship for calculating the effective diffusivity of micro-porous layers. *Int. J. Hydrogen Energy* **40**, 10242–10250 (2015)
- Becker, J., Wieser, C., Fell, S., Steiner, K.: A multi-scale approach to material modeling of fuel cell diffusion media. *Int J Heat Mass Tran* **54**, 1360–1368 (2011)
- Berson, A., Choi, H.-W., Pharoah, J.G.: Determination of the effective gas diffusivity of a porous composite medium from the three-dimensional reconstruction of its microstructure. *Phys. Rev. E* **83**, 026310 (2011)
- Beskok, A., Karniadakis, G.E.: Report: a model for flows in channels, pipes, and ducts at micro and nano scales. *Microscale Thermophys. Eng.* **3**, 43–77 (1999)
- Bhattacharya, S., Gubbins, K.E.: Fast method for computing pore size distributions of model materials. *Langmuir* **22**, 7726–7731 (2006)
- Bird, R.B., Stewart, W.E., Lightfoot, E.N.: *Transport Phenomena*. Wiley, New York (2002)
- Blundell, S.J., Blundell, K.M.: *Concepts in Thermal Physics*. Oxford University Press, Oxford (2009)
- Bruggeman, V.D.: Berechnung verschiedener physikalischer Konstanten von heterogenen Substanzen. I. Dielektrizitätskonstanten und Leitfähigkeiten der Mischkörper aus isotropen Substanzen. *Ann. Phys.* **416**, 636–664 (1935)
- Chai, Z., Huang, C., Shi, B., Guo, Z.: A comparative study on the lattice Boltzmann models for predicting effective diffusivity of porous media. *Int. J. Heat. Mass. Trans.* **98**, 687–696 (2016)
- Chan, C., Zamel, N., Li, X.G., Shen, J.: Experimental measurement of effective diffusion coefficient of gas diffusion layer/microporous layer in PEM fuel cells. *Electrochim. Acta* **65**, 13–21 (2012)
- Chapman, S., Cowling, T.G.: *The Mathematical Theory of Non-uniform Gases*. Cambridge University Press, Cambridge (1953)
- Chen, S., Doolen, G.D.: Lattice Boltzmann method for fluid flows. *Annu. Rev. Fluid Mech.* **30**, 329–364 (1998)
- Chen, L., Wu, G., Holby, E.F., Zelenay, P., Tao, W.-Q., Kang, Q.: Lattice Boltzmann pore-scale investigation of coupled physical-electrochemical processes in c/p and non-precious metal cathode catalyst layers in proton exchange membrane fuel cells. *Electrochim. Acta* **158**, 175–186 (2015)
- Cousins, T.A., Ghanbarian, B., Daigle, H.: Three-dimensional lattice boltzmann simulations of single-phase permeability in random fractal porous media with rough pore-solid interface. *Transp. Porous Med.* **122**, 527–546 (2018)
- Delerue, J., Perrier, E., Yu, Z., Velde, B.: New algorithms in 3D image analysis and their application to the measurement of a spatialized pore size distribution in soils. *Phys. Chem. Earth Part A.* **24**, 639–644 (1999)
- d’Humières, D., Ginzburg, I., Krafczyk, M., Lallemand, P., Luo, L.S.: Multiple-relaxation-time lattice Boltzmann models in three dimensions. *Philos. Trans. R. Soc. Lond. Ser. A Math. Phys. Eng. Sci.* **360**, 437–451 (2002)
- Dreyer, J.A.H., Riefler, N., Pesch, G.R., Karamahmedović, M., Fritsching, U., Teoh, W.Y., Mädler, L.: Simulation of gas diffusion in highly porous nanostructures by direct simulation Monte Carlo. *Chem. Eng. Sci.* **105**, 69–76 (2014)

- El Hannach, M., Singh, R., Djilali, N., Kjeang, E.: Micro-porous layer stochastic reconstruction and transport parameter determination. *J. Power Sources* **282**, 58–64 (2015)
- Ellis, M.W., Von Spakovsky, M.R., Nelson, D.J.: Fuel cell systems: efficient, flexible energy conversion for the 21st century. *Proc. IEEE* **89**, 1808–1818 (2001)
- Fei, F., Fan, J., Jiang, J.: Solid wall effect on the transport coefficients of gases. *Sci. China Phys. Mech. Astron.* **55**, 927–932 (2012)
- Froning, D., Brinkmann, J., Reimer, U., Schmidt, V., Lehnert, W., Stolten, D.: 3D analysis, modeling and simulation of transport processes in compressed fibrous microstructures, using the Lattice Boltzmann method. *Electrochim. Acta* **110**, 325–334 (2013)
- Froning, D., Yu, J., Gaiselmann, G., Reimer, U., Manke, I., Schmidt, V., Lehnert, W.: Impact of compression on gas transport in non-woven gas diffusion layers of high temperature polymer electrolyte fuel cells. *J. Power Sour.* **318**, 26–34 (2016)
- Galinsky, M., Sénéchal, U., Breikopf, C.: The impact of microstructure geometry on the mass transport in artificial pores: a numerical approach. *Model. Simul. Eng.* **2014**, 1–7 (2014)
- Haynes, W.M., Lide, D.R., Bruno, T.J.: *CRC Handbook of Chemistry and Physics*. CRC Press, New York (2012)
- He, X., Guo, Y., Li, M., Pan, N., Wang, M.: Effective gas diffusion coefficient in fibrous materials by mesoscopic modeling. *Int. J. Heat. Mass. Trans.* **107**, 736–746 (2017)
- Hussain, M., Tian, E., Cao, T.-F., Tao, W.-Q.: Pore-scale modeling of effective diffusion coefficient of building materials. *Int. J. Heat. Mass. Trans.* **90**, 1266–1274 (2015)
- Inoue, G., Kawase, M.: Effect of porous structure of catalyst layer on effective oxygen diffusion coefficient in polymer electrolyte fuel cell. *J. Power Sources* **327**, 1–10 (2016a)
- Inoue, G., Kawase, M.: Understanding formation mechanism of heterogeneous porous structure of catalyst layer in polymer electrolyte fuel cell. *Int. J. Hydrogen Energy* **41**, 21352–21365 (2016b)
- Inoue, G., Yokoyama, K., Ooyama, J., Terao, T., Tokunaga, T., Kubo, N., Kawase, M.: Theoretical examination of effective oxygen diffusion coefficient and electrical conductivity of polymer electrolyte fuel cell porous components. *J. Power Sour.* **327**, 610–621 (2016)
- Ismail, M.S., Ingham, D.B., Hughes, K.J., Ma, L., Pourkashanian, M.: Effective diffusivity of polymer electrolyte fuel cell gas diffusion layers: an overview and numerical study. *Int. J. Hydrogen Energy* **40**, 10994–11010 (2015)
- Joshi, A.S., Peracchio, A.A., Grew, K.N., Chiu, W.K.S.: Lattice Boltzmann method for multi-component, non-continuum mass diffusion. *J. Phys. D Appl. Phys.* **40**, 7593–7600 (2007a)
- Joshi, A.S., Peracchio, A.A., Grew, K.N., Chiu, W.K.S.: Lattice Boltzmann method for continuum, multi-component mass diffusion in complex 2D geometries. *J. Phys. D Appl. Phys.* **40**, 2961 (2007b)
- Kärger, J., Ruthven, D.M., Theodorou, D.N.: *Diffusion in Nanoporous Materials*. Wiley, Weinheim (2012)
- Kaviany, M.: *Principles of Heat Transfer in Porous Media*. Springer, New York (1995)
- Kim, S.H., Pitsch, H.: Reconstruction and effective transport properties of the catalyst layer in PEM fuel cells. *J. Electrochem. Soc.* **156**, B673–B681 (2009)
- Kim, S.H., Pitsch, H., Boyd, I.D.: Lattice Boltzmann modeling of multicomponent diffusion in narrow channels. *Phys. Rev. E* **79**, 016702 (2009)
- Krishna, R., van Baten, J.M.: Investigating the validity of the Bosanquet formula for estimation of diffusivities in mesopores. *Chem. Eng. Sci.* **69**, 684–688 (2012)
- Lange, K.J., Sui, P.-C., Djilali, N.: Pore scale simulation of transport and electrochemical reactions in reconstructed PEMFC catalyst layers. *J. Electrochem. Soc.* **157**, B1434 (2010)
- Lange, K.J., Sui, P.-C., Djilali, N.: Pore scale modeling of a proton exchange membrane fuel cell catalyst layer: effects of water vapor and temperature. *J. Power Sour.* **196**, 3195–3203 (2011)
- Lange, K.J., Sui, P.-C., Djilali, N.: Determination of effective transport properties in a PEMFC catalyst layer using different reconstruction algorithms. *J. Power Sour.* **208**, 354–365 (2012)
- Litster, S., Epting, W., Wargo, E., Kalidindi, S., Kumbur, E.: Morphological analyses of polymer electrolyte fuel cell electrodes with nano-scale computed tomography imaging. *Fuel Cells* **13**, 935–945 (2013)
- Luo, L.-S., Girimaji, S.S.: Theory of the lattice Boltzmann method: two-fluid model for binary mixtures. *Phys. Rev. E* **67**, 036302 (2003)
- Ma, Q., Chen, Z.: Lattice Boltzmann simulation of multicomponent noncontinuum diffusion in fractal porous structures. *Phys. Rev. E* **92**, 013025 (2015)
- Nanjundappa, A., Alavijeh, A.S., El Hannach, M., Harvey, D., Kjeang, E.: A customized framework for 3-D morphological characterization of microporous layers. *Electrochim. Acta* **110**, 349–357 (2013)
- Pollard, W.G., Present, R.D.: On gaseous self-diffusion in long capillary tubes. *Phys. Rev.* **73**, 762–774 (1948)
- Shou, D., Fan, J., Mei, M., Ding, F.: An analytical model for gas diffusion through nanoscale and microscale fibrous media. *Microfluid. Nanofluid.* **16**, 381–389 (2014)

- Siddique, N., Liu, F.: Process based reconstruction and simulation of a three-dimensional fuel cell catalyst layer. *Electrochim. Acta* **55**, 5357–5366 (2010)
- Singh, R., Akhgar, A.R., Sui, P.C., Lange, K.J., Djilali, N.: Dual-Beam FIB/SEM characterization, statistical reconstruction, and pore scale modeling of a PEMFC catalyst layer. *J. Electrochem. Soc.* **161**, F415–F424 (2014)
- Tomadakis, M.M., Sotirchos, S.V.: Effective Kundsens diffusivities in structures of randomly overlapping fibers. *AIChE J.* **37**, 74–86 (1991)
- Tomadakis, M.M., Sotirchos, S.V.: Ordinary and transition regime diffusion in random fiber structures. *AIChE J.* **39**, 397–412 (1993)
- Wang, M.: Structure effects on electro-osmosis in microporous media. *J. Heat. Trans. T ASME* **134**, 051020 (2012)
- Wang, M., Pan, N.: Predictions of effective physical properties of complex multiphase materials. *Mater. Sci. Eng. R Rep.* **63**, 1–30 (2008)
- Wang, M., Wang, J., Pan, N., Chen, S.: Mesoscopic predictions of the effective thermal conductivity for microscale random porous media. *Phys. Rev. E* **75**, 036702 (2007a)
- Wang, M., He, J., Yu, J., Pan, N.: Lattice Boltzmann modeling of the effective thermal conductivity for fibrous materials. *Int. J. Thermal Sci.* **46**, 848–855 (2007b)
- Wang, Z., Guo, Y., Wang, M.: Permeability of high-Kn real gas flow in shale and production prediction by pore-scale modeling. *J. Na. Gas Sci. Eng.* **28**, 328–337 (2016)
- Yang, F., Gu, J., Ye, L., Zhang, Z., Rao, G., Liang, Y., Wen, K., Zhao, J., Goodenough, J.B., He, W.: Justifying the significance of Knudsen diffusion in solid oxide fuel cells. *Energy* **95**, 242–246 (2016)
- Yoshida, H., Nagaoka, M.: Multiple-relaxation-time lattice Boltzmann model for the convection and anisotropic diffusion equation. *J. Comput. Phys.* **229**, 7774–7795 (2010)
- Yu, Z., Carter, R.N.: Measurement of effective oxygen diffusivity in electrodes for proton exchange membrane fuel cells. *J. Power Sour.* **195**, 1079–1084 (2010)
- Yu, Z., Carter, R.N., Zhang, J.: Measurements of pore size distribution, porosity, effective oxygen diffusivity, and tortuosity of PEM fuel cell electrodes. *Fuel Cells* **12**, 557–565 (2012)
- Yuan, J.L., Sunden, B.: On mechanisms and models of multi-component gas diffusion in porous structures of fuel cell electrodes. *Int J Heat Mass Tran* **69**, 358–374 (2014)
- Zamel, N., Li, X.: Effective transport properties for polymer electrolyte membrane fuel cells—with a focus on the gas diffusion layer. *Prog. Energy Combust. Sci.* **39**, 111–146 (2013)
- Zamel, N., Becker, J., Wiegmann, A.: Estimating the thermal conductivity and diffusion coefficient of the microporous layer of polymer electrolyte membrane fuel cells. *J. Power Sources* **207**, 70–80 (2012)
- Zhang, X., Gao, Y., Ostadi, H., Jiang, K., Chen, R.: Modelling water intrusion and oxygen diffusion in a reconstructed microporous layer of PEM fuel cells. *Int. J. Hydrogen Energy* **39**, 17222–17230 (2014)